HHS Public Access

Author manuscript

Gene Ther. Author manuscript; available in PMC 2013 August 01.

Published in final edited form as:

Gene Ther. 2013 February ; 20(2): 158–168. doi:10.1038/gt.2012.16.

Three-dimensional multipotent progenitor cell aggregates for expansion, osteogenic differentiation and "in vivo" tracing with AAV vector serotype 6

João R. Ferreira[1,2], **Matthew L. Hirsch**[3], **Li Zhang**[4], **Yonsil Park**[5], **R. Jude Samulski**[3], **Wei-Shou Hu**[6], and **Ching-Chang Ko**[1,7]

[1]School of Dentistry, University of North Carolina-Chapel Hill, Chapel Hill, USA

[2]National Institute of Dental and Craniofacial Research, Bethesda, MD, USA

[3]Gene Therapy Center, University of North Carolina-Chapel Hill, Chapel Hill, USA

[4]Faculty of Stomatology, Capital Medical University, Beijing, China

[5]Interdepartmental Stem Cell Institute, Catholic University of Leuven, Leuven, Belgium

[6]Chemical Engineering and Materials Science, University of Minnesota, Minneapolis, USA

[7]Materials Sciences and Engineering, North Carolina State University, Raleigh, USA

Abstract

Multipotent adult progenitor cells (MAPC) are bone marrow-derived stem cells with a high growth rate suitable for therapeutical applications as three-dimensional (3D) aggregates. Combined applications of osteogenically differentiated MAPC (OD-MAPC) aggregates and adeno-associated viral vectors (AAV) in bone bioengineering are still deferred until information regarding expansion technologies, osteogenic potential, and AAV cytotoxicity and transduction efficiency is better understood. In this study, we tested whether self-complementary AAV (scAAV) can potentially be used as a gene delivery system in a OD-MAPC-based "in vivo" bone formation model in the craniofacial region. Both expansion of rat MAPC (rMAPC) and osteogenic differentiation with dexamethasone were also tested in 3D aggregate culture systems "in vitro" and "vivo". Rat MAPCs (rMAPCs) grew as undifferentiated aggregates for 4 days with a population doubling time of 37h. After expansion, constant levels of Oct4 transcripts, and Oct4 and CD31 surface markers were observed, which constitute a hallmark of rMAPCs undifferentiated stage. Dexamethasone effectively mediated rMAPC osteogenic differentiation by inducing the formation of a mineralized collagen type I network, and facilitated the activation of the wnt/β-catenin, a crucial pathway in skeletal development. To investigate the genetic modification of rMAPCs grown as 3D aggregates prior to implantation, scAAV serotypes 2, 3, and 6 were evaluated. scAAV6 packaged with the enhanced green fluorescent protein expression cassette efficiently mediated long-term transduction (10 days) "in vitro" and "vivo". The reporter

Correspondence should be addressed to J.R.F. : Matrix and Morphogenesis Section, LCDB, NIH/NIDCR, 30 Convent Dr, Room 429, Bethesda, MD 20892-2190 Phone: +1 301 594 4123; Fax: +1 301 402 0897; andraderequicj@nidcr.nih.gov.

All authors reported no conflict of interests.

transduction event allowed the tracing of OD-rMAPC (induced by dexamethasone) aggregates following OD-rMAPC transfer into a macro-porous hydroxyapatite scaffold implanted in a rat calvaria model. Furthermore, the scAAV6-transduced OD-rMAPC generated a bone-like matrix with a collagenous matrix rich in bone specific proteins (osteocalcin and osteopontin) in the scaffold macro-pores 10 days post-implantation. Newly formed bone was also observed in the interface between native bone and scaffold. The collective work supports future bone tissue engineering applications of 3D MAPC cultures for expansion, bone formation, and the ability to genetically alter these cells using scAAV vectors.

INTRODUCTION

Stem cell-based clinical applications require both a large quantity of cells and an effective expansion technology with a reproducible differentiation protocol for bone formation and regeneration of large skeletal defects. Multipotent adult progenitor cells (MAPC) are a bone marrow subpopulation of stem cells characterized by high levels of CD31 and Oct4. This latter marker is crucial for their extensive self-renewal ability as revealed in embryonic stem cells (ESCs).[1] Besides its self-renewal advantage, MAPC also present more homogeneity[1] when compared to mesenchymal stem cells (MSC), and the clinical grade human MAPCs (Multistem®) offer therapeutic relevance as a immunomodulatory treatment tool for certain diseases (ClinicalTrials.gov NCT00677859, NCT00677222).[2] However, little is known about the clinical potential of MAPC to form bone tissue, and also on the phenotypic and genotypic expression pattern during MAPC osteogenic differentiation. Furthermore, combined applications of MAPC and adeno-associated viral (AAV) vectors in bone tissue engineering have been deferred until AAV cytotoxicity and transduction efficiency are thoroughly investigated.

Recently, the rat MAPC (rMAPC) line has been shown to have a high expansion rate when cultured as static three-dimensional (3D) cell aggregates.[3] These cell aggregates retained their pluripotency state for at least 16 days.[3] More importantly, researchers have demonstrated that 3D static aggregate stem cell cultures are robust bioprocesses for MAPC expansion that offer safety advantages over suspension cultures. [3,4] Unlike suspended aggregates, static ESC cultures do not form invasive tumors after “in vivo” transplantation. [4] Moreover, adult stem cells (like MSCs) are known to differentiate in the presence of bone signaling cues, such as dexamethasone and bone morphogenetic protein-2 (BMP-2) through wnt/β-catenin pathways.[5,6] In our preliminary studies with 2D cultures, dexamethasone positively modulated the osteogenic differentiation of rMAPCs, but not exogenous recombinant human BMP-2, a potent osteogenic growth factor. Thus, it would be important to test the reproducibility of dexamethasone osteogenic effects in 3D aggregate systems, since the 3D system better mimics the “in vivo” environment with a higher expansion capability.[3,5] Interestingly, 3D cultures of human ESCs have also been confirmed as a viable alternative to monolayer 2D systems, and possess a significant “in vivo” reproducibility after long-term culture.[7] Therefore, this study focused on investigating rMAPC 3D aggregate static long-term cultures for cell expansion and osteogenic differentiation induced by dexamethasone.

In addition to applications of MAPCs for characterization of bone formation in large skeletal defect models, the therapeutic potential of transgenic MAPCs is also of particular interest. For example, multipotent or differentiated MAPCs could be altered to express or secrete endogenous factors involved in local bone formation, such as BMPs as in other bone fracture healing models.[11] In addition, MAPCs could be labeled (i.e. with the green fluorescent protein) for “in vivo” tracing of cell replication and migration “in vivo”. Currently, viral gene delivery vectors have demonstrated success for the efficient transduction of a wide variety of cell types “in vivo” and “ex vivo”.[12] In particular, recombinant adeno-associated virus (rAAV) offer a broad tropism and have demonstrated success in “in vivo” applications.[12, 13] While several studies have demonstrated MSC transduction by single-strand rAAV serotypes 2, 3 and 6 “in vitro” [14, 15], to our knowledge none have evaluated the transduction of self-complementary rAAV vectors in MAPCs for “in vitro” and/or “in vivo” applications in large calvaria bone defects within a non load-bearing environment. These critical-size large defects (CSD) do not heal by themselves, and therefore, they may need a combination of MAPC-based bone tissue engineering approaches and AAV vector technologies for bone formation to occur.

Thus, our hypotheses test whether a 3D cell culture system can provide a large number of rMAPCs for (1) osteogenic differentiation with dexamethasone supplementation and (2) rAAV-mediated gene transfer for “in vivo” bone formation in calvaria large defects. The transduction efficiency of rAAV serotypes on multipotent and differentiated rMAPCs was investigated and a transgenic reporter used to track rMAPC aggregates “in vivo” in 3D scaffolds in rat calvaria CSD. This “in vitro” 3D culture system may allow the expansion, bone formation, and effective AAV-based gene delivery for “in vivo” bone healing therapies.

RESULTS

1. Expansion and viability of the 3D rMAPC aggregates

Rat MAPC (rMAPC) in 3D aggregates grew steadily up to day 4, increasing from approximately 1,500 up to a mean of 10,548 viable cells per aggregate (Figure 1a). After day 4, the number of viable cells decreased substantially, which is possibly related to the low volume of the growth medium (Figure 1a) ($p<0.001$). Also, the doubling time was consistently 37h through all 4 days of the 3D aggregate culture, and then decreased substantially thereafter. The population of viable cells outstand the dead/damaged cells seen by the large viable-associated red fluorescence 2D plane of the aggregate (Figure 1b). Also, rendering a 3D volume view of the aggregate revealed a large population of viable cells clustered together to form a rounded aggregate as seen in the 2D view (Figure 1b, c).

Similar to the cell aggregate growth curve, there was also an increase in cell aggregate diameter. After the centrifugal settling to the bottom of a well, single cells clustered together to an average diameter of 333μm. Aggregates then increased in size to about 397 μm diameter by 96 h (4 days) after the initial agglomeration ($p<0.001$), and after that point the size of the aggregate remained unchanged (Figure 1d).

After 4 days of rMAPC aggregate expansion, flow cytometry revealed that the cells in the aggregate retain their positive levels for the rMAPC pluripotent marker Oct4 and the rMAPC marker CD31 (Figure S1). This latter marker is highly expressed in undifferentiated MAPC, and therefore is used as an hallmark with Oct4 to confirm rMAPC's undifferentiated state.[1] This was also confirmed at the transcript level, where expression of Oct4 and CD31 remained high at day 4, when compared to baseline levels before expansion started (Figure S1).

2. AAV cytotoxicity and transduction efficiency on rMAPC aggregates

To investigate gene delivery to rMAPCs in the 3D aggregate culture, a self-complementary (sc) CMV-eGFP expression cassette was packaged in capsids previously reported to be capable of MSC transduction.[14] After scAAV-GFP vector transduction at a multiplicity of infection (MOI; viral genomes/cell) of 100, no differences in cell viability were observed between undifferentiated and differentiated rMAPC aggregates for serotypes AAV3 and AAV6(Figure 2a). For AAV2, viability of differentiated rMAPC aggregates was similar to untransduced cells (Figure 2a). However, there was a significant decrease in cell viability when comparing AAV2-treated undifferentiated and differentiated rMAPC cultures ($p \leq 0.01$) (Figure 2a).

In general the transduction efficiency of different scAAV serotypes, as measured by a GFP+ phenotype, was greater in differentiated aggregate cultures compared to undifferentiated cells (Figure 2b). Among the tested serotypes, AAV6 serotype presented the highest percentage of GFP+ cells after 3 days when compared to AAV2 ($p=0.0073$) and to AAV3 ($p=0.0068$). Expression of GFP increased up to day 7 in AAV6-transduced cultures (Figure 3a), and afterwards, cells continued to express GFP through day 14 (Figure 3 b-e).

3. Bone-like matrix derived from dexamethasone-treated rMAPC aggregates

Since effective gene delivery was demonstrated in 3D cultures, we next sought to investigate the effects of dexamethasone on the bone matrix generation and mineralization. Cell/matrix cryo-sections were analyzed after differentiation of rMAPC aggregates was induced by osteogenic media with and without dexamethasone (OMD and OM, respectively) and by basal media (BM) without dexamethasone and osteogenic supplements. Unlike in OM and BM treatment, dexamethasone-treated aggregate cultures were highly immunoreactive to collagen type I antibody and a collagenous fiber network could be observed (Figure 4a). The orange/redness of collagen fibrils could also be appreciated under polarized light after picro-sirius red staining, consistent with a high level of maturation of the collagen (Figure S2c).[16]

Electron microscopy images of the rMAPC aggregate matrices at day 38 confirmed the abundant matrix mineralization in dexamethasone cultures (Figure 4b) indicated by large areas of long spindle-like crystals (white arrows). On demineralized sections at an earlier time point (day 27), few matrix demineralized areas were observed, as well as a densely compacted matrix which possessed regions with typical collagen D-periodicity (data not shown). On the other hand, matrix-formed crystals were scarce and short in length in

cultures grown in the absence of dexamethasone (Figure 4d). In rMAPC aggregate matrices grown in basal medium no crystals were observed (Figure 4f).

All these matrix features in OMD cultures resembled natural bone tissue. On the contrary, aggregate cultures without dexamethasone (both OM and BM cultures) showed poorly mineralized matrices with scarce collagen type I (Figure 4c, e). In addition, all matrices in dexamethasone medium stained poorly for lipid deposits (red deposits stained by Oil red O in Figure S2a) and for proteoglycans (orange/red areas stained by Safranin O in Figure S2b). [6] These observations indicate that dexamethasone-treated rMAPC aggregates committed to an osteogenic phenotype and not to adipogenic or chondrogenic lineages.

4. Dexamethasone increases expression of mesoderm and bone markers in rMAPC aggregates

After undergoing a dexamethasone-enriched osteogenic differentiation protocol for 38 days in 3D cultures, Oct4 mRNA levels in rMAPC decreased significantly to an average ΔCT of approximately 2 compared to baseline levels (Fold change=0.7, Figure 4g) (p=0.019). This observation was consistent with other literature[3] and was seen at a lesser extent in cultures treated without dexamethasone (OM: average ΔCT=3, Fold change=0.9), suggesting that dexamethasone is inducing rMAPC differentiation. The alpha-fetoprotein (Afp) transcript, which is usually upregulated on differentiated cells, was expressed at high levels in osteogenic culture medium without dexamethasone (OM) but without significance and to a lesser degree in dexamethasone-enriched media (OMD) with significance (p<0.01) (Figure S3). At the terminus of the differentiation process, the endothelial-specific marker CD31 was significantly downregulated in both media without dexamethasone (p=0.003928) and with dexamethasone (p=0.035557), ruling out a possible endothelial commitment (Figure 4h). Also, Kdr, a mediator of VEGF-induced endothelial proliferation and differentiation, was found downregulated in dexamethasone-supplemented cultures (Figure 4h). More importantly, mesoderm-specific transcripts such as BMP-2 (p=0.039) and BMP-4 (p=0.015) were found highly upregulated by dexamethasone, and to lesser extent in OM without dexamethasone (Figure 4h). Essential mid- to late-stage osteogenesis markers signaling molecules were assessed, particularly Col1a2, osteopontin (OSP), and osteocalcin (OCN) (Figure 4i). The late bone-specific gene, OCN (Figure 4i), was found highly upregulated with dexamethasone when compared to medium without dexamethasone (p=0.014). Collagen type 1 (Col1a2) and osteopontin (OSP) early bone markers were overexpressed relative to baseline (Figure 4i); however, transcript expression was without significance for Col1a2, perhaps due to the ongoing late stage of bone development (38 days) on dexamethasone culture conditions (OMD). In summary, overexpression of mesodermal and late bone-specific genes in OMD confirmed their osteogenic potential under dexamethasone supplementation in this 3D culture system.

5. Nuclear co-localization of β-catenin increased in rMAPC aggregates treated with dexamethasone

After confirming the osteogenic potential of rMAPC aggregates, we assessed the activation of the wnt/β-catenin pathway, crucial on skeletal development. Expression of nuclear β-catenin was evaluated during the osteogenic differentiation in medium with and without

dexamethasone. To confirm the translocation of the β-catenin to the nucleus and inhibition of β-catenin degradation, the expression of the activated form of GSK3 (*p*-GSK3 Tyr 216/279) that sequesters and negatively regulates β-catenin activation was also assessed. The β-catenin is only activated when a Wnt signal is present and *p*-GSK3 kinase activity is inhibited.[6] Upon activation β-catenin is mainly found free and co-localized with the nucleus, and this was demonstrated only in dexamethasone-differentiated rMAPC cells (Figure 5a). Conversely, in OM without dexamethasone (OM), β-catenin was found outside the nucleus and closely associated with the plasma membrane, which suggests that this molecule is inactive, and therefore, no wnt signaling occured (Figure 5b). These observations were supported by the lack of expression of the β-catenin negative regulator *p*-GSK3 in dexamethasone-treated cultures (Figure 5c) and by its abundant expression in culture media without dexamethasone (OM) (Figure 5d).

6. AAV6 transduction for “in vivo” rMAPC tracing and bone formation

After efficient osteogenic differentiation conditions were set for the aggregates, we then used the AAV6 serotype to both trace the differentiated aggregates “in vivo” and study its effects on bone formation. The ability of scAAV6 to label differentiated rMAPC for “in vivo” tracing was investigated on a macro-porous hydroxyapatite-based 3D scaffold. In these experiments, osteogenically differentiated rMAPC or OD-rMAPC aggregates (dexamethasone-treated at day 38 of differentiation) were transduced with scAAV6-CMV-eGFP at a MOI of 100. On the following day, these transduced aggregates were loaded into macro-porous hydroxyapatite-based scaffolds, which were then implanted in a rat calvaria CSD bone formation model. Four and ten days after “in vivo” implantation of porous scaffolds with AAV6-transduced rMAPC, tracing of transduced cells revealed GFP+ cells on the porous areas around the scaffold materials (Figure 6 a-e). The number of GFP+ cells appeared to be higher at 10 days than at 4 days of post-implantation (Figure 6f).

Importantly, untransduced and AAV6-transduced rMAPCs generated a osteogenic-like tissue expressing late specific bone markers (such as osteopontin and osteocalcin) within the macro-pores of the 3D scaffold after 10 days (Figure 7 a-b, d-e). Furthermore, transplanted AAV6-transduced rMAPCs formed a bone-like collagenous matrix with osteocyte-like cells entrapped in lacunae within the macro-pores (Figure 7g-h). Also, newly formed bone was visualized at the native bone-scaffold interface 10 days after implantation of transduced cells (Figure 7i). These observations indicate that rAAV6 transduction allows for “in vivo” bone formation and mediates stable gene transfer to differentiated rMAPC aggregates, which remains strong post-implantation while not affecting the osteogenic differentiation of rMAPCs. Lastly, Oct4 expression was not detected in GFP+ cells “in vivo” after 10 days, and therefore, the presence of cell growth from day 4 to 10 was not related to the presence of immortalized rMAPC (Figure 8).

DISCUSSION

Stem cell-based approaches are valuable tools not only for the formation of new tissues like bone, but also when used as models of bone disease and to understand bone development. [17, 18, 19] Rat and human MAPCs have been used as cell-based therapies for newly

formed tissues in rodent studies [20, 21], and MAPC-based clinical trials have been initiated to take advantage of MAPCs immunomodulatory effects (ClinicalTrials.gov NCT00677859, NCT00677222). Our current study successfully combined for the first time osteogenically differentiated rat MAPC (OD-rMAPC) and AAV vector mediated gene delivery for the final purpose of bone formation in a calvaria critical-size defect (CSD) model.

Rat calvaria “in vivo” CSD models require a large number of cells, which often rely on growth in cell scale-up bioprocesses.[5, 22, 23] Despite several innovations in these robust bioprocesses, progress has been slow due to cellular heterogeneity including karyotypic abnormalities associated with prolonged “ex vivo” culture times, which make stem cells unfit for clinical use.[24, 25, 26] However, in this studywe used a cell line (rMAPCs) with high self-renewal ability and homogeneity, and thus we were able to expand rMAPCs on static 3D aggregate culture systems for a short time period (4 days). Recently, rMAPC have shown to possess a high expansion rate with a doubling time of about 23h in 3D suspension cultures.[3] In our study, the doubling time was consistently 37h through all 4 days of the 3D aggregate culture. The lower doubling time reported by Subramanian et al.[3] is probably related with the different cell counting protocol used. Determining the viable cell population was a more appropriate approach in this study, since poor diffusion of oxygen and essential nutrients to the center of the aggregate has been found to compromise cell survival and increase Oct4 mRNA levels.[4] Though, the expansion observed here as cell aggregates did not compromise the viability of the cells (approximately 85-95% of viability/aggregate), particularly in the center of the aggregate as seen by the large viable-associated red fluorescence (Figure 1b). In the periphery of the aggregate few nonviable cells were observed, but those were attached to the bottom of the well and not clustered to the aggregate. The 3D volume view of the aggregate revealed a large number of viable cells clustered together to form a robust rounded aggregate of about 400 μm in diameter. At the end of expansion, cells in aggregates retained their initial rMAPC undifferentiated state, as seen in other studies.[3]

After an appropriate expansion method was found, we tested the osteogenic potential of rMAPC aggregates under different media conditions with and without dexamethasone. Dexamethasone appears to drive commitment of rMAPC aggregates to an osteogenic phenotype and not to chondrogenic, adipogenic or endothelial lineages, since: i) matrices had little proteoglycans and lipids deposits (Figure S2), and ii) differentiated cells had the endothelial cell marker CD31 downregulated at the mRNA and protein levels (Figure 4h). At the transcriptional level, dexamethasone also significantly increased the expression of late bone-specific markers (osteocalcin) and endogenous osteogenic growth factors (BMP-2 and BMP-4) (Figure 4h). Formation of collagen type I and of large areas of long spindle-like crystals and crystal nucleation was seen on matrices when dexamethasone was supplemented, which indicates that normal calcification occurred (Figure 4a-b). Dystrophic (or abnormal) calcification has been reported elsewhere when organic phosphates are added to osteogenic culture medium.[27, 28] On the other hand, our cultures without dexamethasone had the crystal nucleation and formation drastically impaired (Figure 4c-f).

In preliminary monolayer culture studies, dexamethasone stimulated rMAPC to form a bone-like matrix in vitro and increased ALP activity at early stages. In this study,

dexamethasone-enriched medium induced the translocation of the β-catenin molecule to the nucleus during rMAPC differentiation (Figure 5a), suggesting the activation of the wnt/β-catenin pathway. Elucidating the role of dexamethasone in the activation of the β-catenin pathway is important, since this pathway was found to be essential in skeletal development, and stem cell fate.[9, 10, 29, 30] Here in 3D aggregate cultures, we found that dexamethasone also increased the nuclear β-catenin at the terminus of rMAPC osteogenic differentiation, like in MSCs.[31] The free translocation of β-catenin to the nucleus was confirmed by the absence of GSK3 (Figure 5c). Besides the presence of wnt, the β-catenin signaling requires the inhibition of GSK3 kinase activity, since the active form of GSK3 targets β-catenin for proteasomal degradation.[30] The GSK3-β-catenin degradation complex is activated when a specific tyrosine is phosphorylated at GSK3.[32, 33] Conversely, in medium without dexamethasone (OM), the β-catenin was not found in the nucleus in the presence of an abundant *p*-GSK3 kinase, which targets β-catenin for degradation and restricts its nuclear translocation. The concomitant activation of the β-catenin pathway and inhibition of the GSK3 kinase activity has been reported and extensively reviewed in literature.[30, 34, 35, 37] The interaction of the BMP and wnt pathways seems to be particularly complex in bone development.[31, 37, 38] The existence of different levels of crosstalk between BMP and wnt has been recently confirmed during the differentiation of the Drosophila mesoderm and of other stem cell lineages.[31, 37, 39] Nevertheless, these complex interactions are far away from being fully understood and further research is mandatory for later bone regeneration applications.

AAV vectors are proving to be increasingly effective because of their superior safety profile and “in vivo” sustained transgene expression[40, 41], including their ability to transduce nondividing primary cells[42] and certain adult stem cell lineages.[14, 15, 43] The results present herein suggest that safe, efficient, and long-term OD-rMAPC aggregate transduction is feasible through 14 days “in vitro” and 10 days “in vivo” for rat calvaria defects (endpoints of the study) through the use of scAAV6 vectors (Figures 3 and 6). Importantly, gene transfer with self-complementary AAV6 (scAAV6) didn’t affect the osteogenic differentiation of rMAPC or the proliferation of these osteoblast-like cells (Figure 7). Undifferentiated aggregates displayed reduced transduction efficiency with the three analyzed scAAV serotypes, and an increase cytotoxic trend, particularly with scAAV2 (Figure. 2). To our knowledge, this is the first report comparing the scAAV transduction efficiency in undifferentiated versus differentiated MAPC using a 3D culture system. As previously mentioned, the therapeutical potential of human MAPC cells is currently being tested in clinical trials.[2] This fact plus the stable transduction efficiency seen here with scAAV6, makes the MAPC 3D aggregate system an ideal cell-based therapy for AAV6-mediated gene delivery. Compared to previous literature[14], levels of AAV6 transduction efficiency on rMAPC were significantly higher (15-27% up to day 7) at lower MOIs (100) than with human MSCs at MOIs of 10^7 (<0.5%). Yet, further studies are needed focusing on AAV transduction efficiency of human MAPCs because efficient gene transfer decreases significantly from nonhuman primates to humans when using marrow-derived adult stem cells (MSCs).[14] More interestingly, our 3D hydroxyapatite macro-porous scaffolds loaded with untransduced and transduced OD-rMAPC aggregates generated a bone-like tissue 10 days after implantation in calvaria CSD models that do not heal by themselves (Figure 7).

These findings indicate this scAAV6 technology could be used with rMAPC for future bone regeneration approaches with porous 3D hydroxyapatite-based scaffolds. Nevertheless, optimal conditions for the complete regeneration of this calvaria defect model by MAPCs have yet to be established, as well as for load-bearing defect models (e.g. femur).

In conclusion, the results demonstrate that rMAPC in this 3D culture system can be a feasible model to effectively generate valuable sources of: (1) rMAPCs, and (2) OD-rMAPCs intended for transplantation with macro-porous 3D scaffolds for “in vivo” bone formation in calvaria. When transplanted to scaffolds, the scAAV6-transduced and untransduced OD-rMAPC can form a bone-like tissue at initial bone healing stages. Future advantages of this model include 1) to engineer bone tissues using a MAPC-based scaffold construct after longer implantation periods, and 2) to study bone development, including the crosstalk levels between BMP and wnt pathways.

MATERIALS and METHODS

1. MAPC isolation and maintenance

Multipotent adult progenitor cells (MAPCs) derived from rat bone marrow (rMAPC) were isolated and characterized at the University of Minnesota Stem Cell Institute according to a well-established protocol.[44,45] Briefly, six to ten million cells were plated in MAPC growth medium. The plates were incubated in a humidified incubator at 37°C with 5% O_2 and 5–6% CO_2. After 4 weeks of culture, cells were depleted of CD45 and Ter119 using magnetic microbeads and the remaining cells were seeded. After 3–14 weeks, cells with a typical spindle-shaped rMAPC morphology appeared. To confirm that these clones were in fact MAPC, the level of Oct4 mRNA was determined using quantitative RT-PCR and the presence of CD31, typical for rMAPC was analyzed by fluorescence-activated cell sorting (FACS). Once a cell line with rMAPC phenotype (*Oct4* mRNA at ΔCt of 4–6, and CD31 positive) was derived, a large frozen working cell bank was prepared. The characteristics of the putative rMAPC were then evaluated (endothelial, hepatocyte, and neural precursor-like differentiation; and further transcriptome phenotype) as previously described.[1] During subsequent cell expansion/maintenance, quality control studies were performed up to passage 30. Rat MAPC cells from passage 20 were used for all the experiments of the present study.

2. rMAPC Growth and Osteogenic Medium

Briefly, rMAPC growth medium consisted of a 60/40 (v/v) mixture of low glucose DMEM (Gibco, CA) and MCDB-201 (Sigma, MO) supplemented with 0.026 μg/mL ascorbic acid 3-phosphate (Sigma), linoleic acid bovine serum albumin (LA-BSA, Sigma) (103 μg/mL BSA and 8.13 μg/mL linoleic acid), insulin-transferrin-selenium (ITS, Sigma) (final concentration 10 μg/mL insulin, 5.5 μg/mL transferrin, 0.005μg/mL sodium selenite), 0.02 μg/mL dexamethasone (Sigma), 4.3 μg/mL β-mercaptoethanol and 2% (v/v) qualified fetal bovine serum (FBS, Hyclone, IL). Three growth factors were also added to the media: human platelet derived growth factor (PDGF-BB, R&D Systems, MN) (10 ng/mL), mouse epidermal growth factor (EGF, Sigma) (10 ng/mL), and mouse leukemia inhibitory factor

(LIF) (103 Units/mL) (Chemicon, ESGRO). All media were also supplemented with 100 IU/mL penicillin and 100 μg/mL streptomycin (Lonza, MD).

Basal medium (BM) composition consisted of 60/40 (v/v) mixture of low glucose DMEM and MCDB-201 supplemented with LA-BSA (103 μg/mL BSA and 8.13 μg/mL linoleic acid), ITS (final concentration 10 μg/mL insulin, 5.5 μg/mL transferrin, 0.005μg/mL sodium selenite), 4.3 μg/mL β-mercaptoethanol and 10% FBS. Basal media did not have dexamethasone supplementation. Osteogenic medium (OM) was composed of BM with the addition of 10mM of β-glycerophosphate (Sigma) and ascorbic acid at 0.2mM (Sigma) with or without dexamethasone supplementation at 10^{-7}M (OMD and OM, respectively).[45]

3. Cell culture systems

Rat MAPCs (rMAPC) were cultured either as three-dimensional (3D) aggregates or as monolayer (2D) cell culture systems in an incubator at 37°C, 5% CO_2 and O_2 while in growth media, and when differentiation media (OMD, OM, BM) was supplemented, cell cultures were changed to normal O_2 levels.

For the 3D aggregate system, 1-2×10^3 MAPC cells were seeded in suspension with MAPC growth medium in 96-well rounded bottom ultra-low attachment plates (Costar), using a modification of a forced aggregation method previously reported.[3, 46] Cells in suspension were centrifuged at 1400 rpm for 4 minutes to allow cells to settle to the bottom of the well and form aggregates over time. Aggregates were allowed to grow for 5 days, and cell viability and diameter of aggregates was monitored at day 1, 2, 3, 4 and 5 (see protocol below). Then, at day 4 ten 3D aggregates were transferred to each well on 24-well ultra-low attachment plates (Costar), and the medium was completely changed to either BM, OM and OM with dexamethasone (OMD). OM and BM had no dexamethasone supplementation. Medium change took place every 2-3 days. All of these 3 culture conditions (BM, OM and OMD) were evaluated for osteogenic differentiation. Differentiation was terminated at both 27 and 38 days.

For the 2D monolayer cultures, 8×10^4 rMAPCs were seed with rMAPC growth medium in 24-well flat plates with regular attachment properties (Costar). Cells were allowed to grow for 4-5 days until they reach the 80-90% of confluency for mesodermal differentiation. Then, growth medium was completely replaced by either OMD, OM or BM conditions, to study the osteogenic potential of the rMAPC aggregates using these three culture conditions. Media change took place every 2-3 days. All these culture conditions (OM and OMD) were evaluated for osteogenic differentiation. Differentiation was terminated at both 21 and 42 days.

4. Cell Viability and rMAPC 3D Aggregate Diameter

During the 4 days of rMAPC aggregate growth, cell viability and proliferation in the aggregates was assessed by a CellTiter 96 Aqueous One Solution assay kit (Promega, WI) according to the manufacturer. Briefly, this kit contains a MTS compound that is bioreduced by cells into a colored formazan product. The quantity of formazan product was measured by the amount of 490nm of absorbance which is directly proportional to the number of living cells in culture. In order to perform the assay, 20ul of CellTiter 96 solution was added

to the media with gentle shaking. Plates were then placed in incubator for about 2h at 37°C, 5% CO_2 and 5% O_2. Background absorbance from negative controls (without cells) was typically 0.206-0.216 for all wells; this average background was subtracted from all absorbance values of experimental groups for normalization. Eight biological replicates were run at day 0, 2, 4 and 5. The cell number was determined by performing cell titration.

A Live/Dead® Cell Vitality Assay C12-resazurin/SYTOX® Green kit (L34951, Molecular Probes, Eugene, OR) was used to visualize the cell viability status within the 3D aggregate according to the manufacturer. Briefly, the aggregates were incubated at 37°C for 15 minutes with the kit working solutions. Metabolically active cells will stain red fluorescent color, and stain damaged or dead cells in green. Fluorescence was observed by microscopy with bright field, TRITC and FITC filters with Nikon Eclipse Ti-U camera (Nikon, Japan), and Nikon NIS Elements software was used to render the 2D and 3D images of the aggregate. The diameter of five cell aggregates was recorded from day 0 to 5 with light microscopy using previous Nikon camera and software.

5. Intracellular Staining for Oct4 and CD31 by Flow Cytometry

The protocol used for MAPC characterization by flow cytometry has been published elsewhere.[1, 45] Briefly, after 4 days of MAPC aggregate expansion (in growth media), cells were harvested by trypsinization of aggregates were washed with and suspended in PBS with 3% (v/v) serum at 100,000 cells per tube. After fixing and blocking for 1h, cells were incubated with antibodies against *Oct4*, CD31 and CD44 to confirm whether cells retained the levels of these undifferentiated rMAPC markers.

6. Histological analysis of 3D aggregate matrices

On day 27 and 38, cell/matrix layers from 3D aggregate and 2D cultures, were washed with calcium-free PBS 1x and fixed. Cryosections with approximately 5μm thickness were made from the rMAPC aggregate matrices. For collagen maturation, matrix cryosection slides were stained for 1h in 0.1% solution of Sirius red dissolved in aqueous saturated picric acid (Electron Microscopy Sciences, PA) for collagen identification.[16] Slides were dehydrated in gradient ethanol, followed by xylene treatment and resin mounted. Stained cell/matrix layers were visualized and photographed with a Nikon Eclipse Ti-U with an Olympus DP70 camera (Japan) on polarized light.

For cartilage tissue analysis, cryosections were stained using a Safranin O staining protocol. Briefly, cryosection slides were stained with Weigert's iron hematoxylin working solution for 10 minutes, washed in water , stained with Fast Green solution for 5 minutes, rinsed quickly with 1% acetic acid solution for 10 –15 seconds, and stained in 0.1% safranin O solution for 5 minutes. Dehydration followed and mounting followed.

Lipid deposition in cell matrices was evaluated using Oil Red O staining protocol after fixation of cryosection slides. Briefly, cell/matrices layers were rinsed with 60% isopropanol, stained with freshly prepared Oil Red O working solution 15 min (Electron Microscopy Sciences, PA), rinse with 60% isopropanol and stained with Harris Hematoxylin for nuclei counterstain. All cell/matrices layers were visualized under light microscopy

(Nikon Eclipse Ti-U, Japan with an Olympus DP70 camera). Matrices stained with Picro-sirius Red solution were observed under polarized light to view collagen organization and maturation. All experiments were run in triplicate.

7. Immunohistochemistry

Rat MAPC aggregates/matrix cryosections were fixed with 4% paraformaldehyde (PFA), rinsed, endogenous peroxidase activity was inhibited by incubating for 30 min with 0.3% H_2O_2 in 100% methanol, rehydrated, and transferred to PBS–Triton solution.

For collagen type I, avidin/biotin activity was blocked in the cryosections with Avidin-Biotin kit (Dako, CA), rinsed thrice with PBS plus Triton X and unspecific antibody binding sites were blocked for 30 min with 0.4% fish skin gelatin in PBS. Then, cryosections were incubated overnight at 4°C with rabbit primary antibody against rat collagen type I (NB600-408, Novus Biologicals, CO), rinsed thrice, and incubated with secondary biotinylated goat anti-rabbit IgG antibody (NB730-B, Novus Biologicals) for 30 min at RT. The cell/matrix layer was incubated in ABC complex (Vector Laboratories, CA) according to the manufacturer's protocol, rinsed thrice, and DAB Chromogen solution (Dako, CA) was added to the matrix layer for 5-20 minutes until brown color developed. Positive controls with collagen type I matrices produced by osteoprogenitor cultures (MC3T3-E1) and negative controls containing a gelatin substrate were also stained. Cell/matrices layers were visualized under light microscopy.

For β-catenin and active form of GSK3α/β immunostaining, cryosections were incubated overnight at 4°C with either goat primary antibody against rat β-catenin (C-18) (sc-1496, Santa Cruz Biotechnology, CA) or p-GSK3α/β (Tyr279/Tyr216) (sc-11758, Santa Cruz), rinsed thrice, and incubated with secondary donkey anti-goat DyLight649-conjugated IgG antibody (705-496-147, Jackson ImmunoResearch, PA) for 30 min at RT. Then, cryosections were counterstained with DAPI nuclei kit (Millipore, Billerica, MA) for 5 min. Sections with primary rat osteoblast cultures were used as positive controls to view β-catenin translocation from the plasma membrane to the nucleus. β-catenin, GSK3α/β and nuclei were observed under fluorescent microscopy (Nikon Eclipse Ti-U with Nikon Digital sight DS-Qi1Mc camera, Japan) with TRITC and DAPI filters, respectively; photos were taken for each filter and then merged together.

8. Transmission Electron Microscopy

On day 27 and 38 of differentiation, 3D aggregate cells/matrices were washed twice with PBS 1X and fixed in 2.5% glutaraldehyde, 2% paraformaldehyde in 0.1M sodium cacodylate buffer (pH 7.4). For decalcification, a 0.1M EDTA solution was used for 2 days buffered with 0.15M sodium phosphate, at pH 7.4, 4°C. Then samples were post-fixed in potassium ferrocyanide reduced osmium (1% osmium tetroxide/1.25% potassium ferrocyanide/0.15M sodium phosphate, pH 7.4) for 1 h. For undecalcified samples, after the ethanol dehydration series, propylene oxide was used as an intermediate solvent, followed by incubation in a solution of propylene oxide and Polybed 812 resin for 2 h, samples stayed overnight in Polybed 812 resin, and then polymerization was achieved in the tube for 24 hours at 60°C. Ultrathin sections with 70nm thickness were cut, stained with uranyl acetate

and lead citrate, and observed using a LEO EM-910 transmission electron microscope operating at 80kV (Carl Zeiss SMT, Peabody, MA), and images were taken at 2,000-50,000X using a Gatan Orius SC1000 CCD camera with Digital Micrograph 3.11.0 (Gatan, Inc., Pleasanton, CA) at the Microscopic Services Laboratory (MSL) at the University of North Carolina. Matrices/cell layer sections from differentiated osteoblast-like murine-derived clonal MC3T3-E1 cell lines were used as a positive control for comparison purposes with OD-rMAPC.

9. Gene Expression Arrays

Rat MAPCs were collected from aggregate cultures at baseline (day 0), day 4 of growth, and day 38 of differentiation in three media conditions (BM, OM and OMD) with TRIzol reagent (Invitrogen) for total RNA extraction, according to manufacturer protocol. Total RNA purification was performed with a RNeasy Mini Kit (Qiagen). Reverse transcription to cDNA was achieved by mixing 500ng of total RNA with a first strand cDNA synthesis mix (from RT^2 First Strand Kit C-03, SABiosciences, MD), based on established manufacturer protocol. Real-time PCR reaction was accomplished by adding RT^2 qPCR Master Mix (RT^2 SYBR Green/ROX qPCR Master Mix, SABiosciences, MD) to the first strand cDNA synthesis reaction at room temperature; the cocktail mix was dispensed into a 96-well plate rat osteogenesis customized RT^2 Profiler PCR array (array CAPR09685, SABiosciences, MD), which was then run in a 7500 Real Time PCR System. Three biological replicates were analyzed for each experimental group, and the fold change was calculated relative to day 0 (baseline) and normalized to the mean expression of three house-keeping genes (Rpl13a, Ldha, Actb). If fold change >1, this indicates an up-regulation of the gene; if fold change <1, it will indicate a down-regulation. The SABiosciences web-based platform was used for PCR data analysis. The mRNA expression of the following genes was analyzed: Smad1, Runx2, Sox9, Osx (osterix), Col1a2 (collagen type I alpha 2 chain), OSP (osteopontin), OCN (osteocalcin), BMP-2, *Oct4*, BMP-4, Kdr, Afp, and CD31.

10. In vitro AAV transduction

Recombinant self-complementary AAV-CMV-eGFP vectors serotypes 2, 3B and 6 were produced using our previously described triple transfection protocol in human embryonic kidney cells.[12, 47] Following transfection, the nuclear lysate was fractionated based on density using cesium chloride centrifugation.[47] Fraction samples were then digested with DNAseI, subsequently followed by proteinase K digestion, and the remaining viral genomes were denatured in a sodium hydroxide solution as described.[47] Alkaline gel electrophoresis and southern blotting were used to identify fractions with self-complementary genomes, which were then pooled and dialyzed in PBS.[48] The viral titer was then determined by quantitative PCR using the following GFP primer set: forward primer, 5-AGCAGCACGACTTCTTCAAGTCC-3′, and the reverse primer 5-TGTAGTTGTACTCCAGCTTGTGCC-3. The final titer was then verified by southern blotting. Cultures with 3D undifferentiated aggregates (after 4 days of aggregate expansion in GM) and 3D dexamethasone-differentiated 3D aggregates (after 15 days in OM plus dexamethasone) in 24 ultra-low attachment wells were incubated for 3, 7 and 14 days with serotypes AAV2-GFP, AAV3B-GFP and AAV6-GFP at multiplicities of infection (MOI; viral genomes/cell) of 100. After trypsinization, cell viability was assessed after 72h of

transduction using the CellTiter 96 Aqueous One Solution assay kit as recommended (Promega). Also, quantification of rAAV transduction efficiency was performed by evaluating GFP positive cells using flow cytometry with dead cell exclusion by gate region. Transduction efficiency was monitored for 14 days using fluorescence microscopy and photos were taken with FITC filter using the previously mentioned Nikon apparatus.

11. “In vivo” tracing and bone formation with AAV6-GFP-transduced OD-rMAPC aggregates

Three-dimensional macro-porous hydroxyapatite-based scaffolds (diameter 8mm and thickness 2 mm) developed previously in our lab[48] were used to carry dexamethasone-treated osteogenically differentiated rMAPC (OD-rMAPC) aggregates after rAAV6 transduction at MOI 100 into an “in vivo” bone large defect model in calvaria. The defect consisted in a 8-mm-diameter calvaria critical-size defect, which has been described.[49] Eleven- to thirteen-week-old Sprague-Dawley rats (Charles River, Wilmington, MA) served as recipients of the rMAPC aggregate-loaded scaffolds. Rats were anesthetized and an 8-mm-diameter defect was created on the calvaria bone using a dental drill. Rats were divided into scaffold groups with untransduced cell aggregates; and groups with AAV6-GFP transduced aggregates.

Four and ten days after surgery, rats were euthanized and the specimens were retrieved for decalcification and immunohistological examinations with antibodies against rat GFP, Oct4, osteopontin, osteocalcin and rabbit IgG (negative isotype CTL). DAB chromogen solution (Dako, CA) was added until brown color developed. Counterstaining with nuclear hematoxylin or alcian blue was also performed. Number of GFP+ cells was counted in 5 random fields in each defect using a microscopy grid of 400×400um. Total of cells was calculated towards a total defect area of 33.6mm^2. Decalcified specimens were also evaluated microscopically for the formation of bone-like matrix and collagen at the hydroxyapatite-based scaffold macro-pores and at the native bone-scaffold interface using hematoxylin-eosin and Masson’s Trichrome histological staining. The experimental protocol for all animal care and use in this study was reviewed and approved by the Institutional Animal Care and Use Committee of the University of North Carolina at Chapel Hill.

12. Statistics

Student t-tests were performed in all assays, except for gene expression data, where one-way ANOVA analysis was used for multiple statistical comparisons using JMP9 software (SAS Institute, NC). Statistical significance was defined at $p<0.05$.

Supplementary Material

Refer to Web version on PubMed Central for supplementary material.

ACKNOWLEDGMENTS

We thank Sandra Horton at North Carolina State University for processing “in vivo” tissue specimens for immunohistochemistry and Victoria Madden at UNC Microscopy Services Laboratory for processing in vitro cell matrices for electron microscopy. Also, we would like to acknowledge Dr. Ganokon Urkasemsin for her contribution towards the statistical analysis of this project. Joäo Ferreira was supported by the doctoral fellowship

of FCT-Portuguese Foundation for Science and Technology (SFRH/BD/36841/2007). This work was supported in part by grants from the: NIH/NIDCR (K08DE018695), NC Biotech Center, American Association for Orthodontist Foundation awarded to C.-C.K.; Northwest Genome Engineering Consortium pilot awarded to M.L.H.; and Wellstone (5U54AR056953) and NIH (5R01AI072176) awarded to R.J.S.

REFERENCES

1. Ulloa-Montoya F, Kidder BL, Pauwelyn KA, Chase LG, Luttun A, Crabbe A, Geraerts M, Sharov AA, Piao Y, Ko MS, Hu WS, Verfaillie CM. Comparative transcriptome analysis of embryonic and adult stem cells with extended and limited differentiation capacity. Genome Biol. 2007; 8:R163. [PubMed: 17683608]
2. Roobrouck VD, Clavel C, Jacobs SA, Ulloa-Montoya F, Crippa S, Sohni A, Roberts SJ, Luyten FP, Van Gool SW, Sampaolesi M, Delforge M, Luttun A, Verfaillie CM. Differentiation potential of human postnatal mesenchymal stem cells, mesoangioblasts, and multipotent adult progenitor cells reflected in their transcriptome and partially influenced by the culture conditions. Stem Cells. 2011; 29:871–882. [PubMed: 21433224]
3. Subramanian K, Park Y, Verfaillie CM, Hu WS. Scalable expansion of multipotente adult progenitor cells as three-dimensional cell aggregates. Biotechnol. Bioeng. 2011; 108:364–375. [PubMed: 20830682]
4. Taiani JT, Krawetz RJ, Zur Nieden NI, Wu Y Elizabeth, Kallos MS, Matyas JR, Rancourt DE. Reduced differentiation efficiency of murine embryonic stem cells in stirred suspension bioreactors. Stem Cells Dev. 2010; 19:989–998. [PubMed: 19775198]
5. Hong L, Sultana H, Paulius K, Zhang G. Steroid regulation of proliferation and osteogenic differentiation of bone marrow stromal cells: a gender difference. J. Steroid Biochem. Mol. Biol. 2009; 114:180–185. [PubMed: 19429449]
6. zur Nieden NI, Kempka G, Rancourt DE, Ahr HJ. Induction of chondro-, osteo- and adipogenesis in embryonic stem cells by bone morphogenetic protein-2: effect of cofactors on differentiating lineages. BMC Dev. Biol. 2005; 5:1–15. [PubMed: 15673475]
7. Arpornmaeklong P, Brown SE, Wang Z, Krebsbach PH. Phenotypic characterization, osteoblastic differentiation, and bone regeneration capacity of human embryonic stem cell-derived mesenchymal stem cells. Stem Cells Dev. 2009; 18:955–968. [PubMed: 19327009]
8. Hong D, Chen HX, Xue Y, Li DM, Wan XC, Ge R, Li JC. Osteoblastogenic effects of dexamethasone through upregulation of TAZ expression in rat mesenchymal stem cells. J. Steroid Biochem. Mol. Biol. 2009; 116:86–92. [PubMed: 19460432]
9. Boyden LM, Mao J, Belsky J, Mitzner L, Farhi A, Mitnick MA, Wu D, Insogna K, Lifton RP. High bone density due to a mutation in LDL-receptor-related protein 5. N. Engl. J. Med. 2002; 346:1513–1521. [PubMed: 12015390]
10. Etheridge SL, Spencer GJ, Heath DJ, Genever PG. Expression profiling and functional analysis of Wnt signaling mechanisms in mesenchymal stem cells. Stem Cells. 2004; 22:849–860. [PubMed: 15342948]
11. Yazici C, Takahata M, Reynolds DG, Xie C, Samulski RJ, Samulski J, Beecham EJ, Gertzman AA, Spilker M, Zhang X, O'Keefe RJ, Awad HA, Schwarz EM. Self-complementary AAV2.5-BMP2-coated Femoral Allografts Mediated Superior Bone Healing Versus Live Autografts in Mice With Equivalent Biomechanics to Unfractured Femur. Mol. Ther. 2011; 19:1416–25. [PubMed: 21206485]
12. McCarty DM, Fu H, Monahan PE, Toulson CE, Naik P, Samulski RJ. Adeno-associated virus terminal repeat (TR) mutant generates self-complementary vectors to overcome the rate-limiting step to transduction "in vivo". Gene Ther. 2003; 10:2112–2118. [PubMed: 14625565]
13. Gao R, Yan X, Zheng C, Goldsmith CM, Afione S, Hai B, Xu J, Zhou J, Zhang C, Chiorini JA, Baum BJ, Wang S. AAV2-mediated transfer of the human aquaporin-1 cDNA restores fluid secretion from irradiated miniature pig parotid glands. Gene Ther. 2011; 18:38–42. [PubMed: 20882054]
14. Chng K, Larsen SR, Zhou S, Wright JF, Martiniello-Wilks R, Rasko JE. Specific adeno-associated virus serotypes facilitate efficient gene transfer into human and non-human primate mesenchymal stromal cells. J. Gene Med. 2007; 9:22–32. [PubMed: 17154338]

15. Stender S, Murphy M, O'Brien T, Stengaard C, Ulrich-Vinther M, Soballe K, Barry F. Adeno-associated viral vector transduction of human mesenchymal stem cells. Eur. Cell. Mater. 2007; 13:93–9. discussion 99. [PubMed: 17538898]
16. Montes GS, Junqueira LC. The use of the Picrosirius-polarization method for the study of the biopathology of collagen. Mem. Inst. Oswaldo Cruz. 1991; 86(Suppl 3):1–11. [PubMed: 1726969]
17. Triffitt JT. Osteogenic stem cells and orthopedic engineering: summary and update. J. Biomed. Mater. Res. 2002; 63:384–389. [PubMed: 12115744]
18. Mauney JR, Volloch V, Kaplan DL. Role of adult mesenchymal stem cells in bone tissue engineering applications: current status and future prospects. Tissue Eng. 2005; 11:787–802. [PubMed: 15998219]
19. Kulterer B, Friedl G, Jandrositz A, Sanchez-Cabo F, Prokesch A, Paar C, Scheideler M, Windhager R, Preisegger KH, Trajanoski Z. Gene expression profiling of human mesenchymal stem cells derived from bone marrow during expansion and osteoblast differentiation. BMC Genomics. 2007; 8:70. [PubMed: 17352823]
20. Ji KH, Xiong J, Fan LX, Hu KM, Liu HQ. Rat marrow-derived multipotent adult progenitor cells differentiate into skin epidermal cells "in vivo". J. Dermatol. 2009; 36:403–409. [PubMed: 19583688]
21. Dimomeletis I, Deindl E, Zaruba M, Groebner M, Zahler S, Laslo SM, David R, Kostin S, Deutsch MA, Assmann G, Mueller-Hoecker J, Feuring-Buske M, Franz WM. Assessment of human MAPCs for stem cell transplantation and cardiac regeneration after myocardial infarction in SCID mice. Exp. Hematol. 2010; 38:1105–1114. [PubMed: 20621157]
22. Kehoe DE, Jing D, Lock LT, Tzanakakis ES. Scalable stirred-suspension bioreactor culture of human pluripotent stem cells. Tissue Eng. Part A. 2010; 16:405–421. [PubMed: 19739936]
23. King JA, Miller WM. Bioreactor development for stem cell expansion and controlled differentiation. Curr. Opin. Chem. Biol. 2007; 11:394–398. [PubMed: 17656148]
24. Buzzard JJ, Gough NM, Crook JM, Colman A. Karyotype of human ES cells during extended culture. Nat. Biotechnol. 2004; 22:381–2. author reply 382. [PubMed: 15060545]
25. Maitra A, Arking DE, Shivapurkar N, Ikeda M, Stastny V, Kassauei K, Sui G, Cutler DJ, Liu Y, Brimble SN, Noaksson K, Hyllner J, Schulz TC, Zeng X, Freed WJ, Crook J, Abraham S, Colman A, Sartipy P, Matsui S, Carpenter M, Gazdar AF, Rao M, Chakravarti A. Genomic alterations in cultured human embryonic stem cells. Nat. Genet. 2005; 37:1099–1103. [PubMed: 16142235]
26. Draper JS, Smith K, Gokhale P, Moore HD, Maltby E, Johnson J, Meisner L, Zwaka TP, Thomson JA, Andrews PW. Recurrent gain of chromosomes 17q and 12 in cultured human embryonic stem cells. Nat. Biotechnol. 2004; 22:53–54. [PubMed: 14661028]
27. Bonewald LF, Harris SE, Rosser J, Dallas MR, Dallas SL, Camacho NP, Boyan B, Boskey A. von Kossa staining alone is not sufficient to confirm that mineralization in vitro represents bone formation. Calcif. Tissue Int. 2003; 72:537–547. [PubMed: 12724828]
28. Declercq HA, Verbeeck RM, De Ridder LI, Schacht EH, Cornelissen MJ. Calcification as an indicator of osteoinductive capacity of biomaterials in osteoblastic cell cultures. Biomaterials. 2005; 26:4964–4974. [PubMed: 15769532]
29. Gong Y, Slee RB, Fukai N, Rawadi G, Roman-Roman S, Reginato AM, Wang H, Cundy T, Glorieux FH, Lev D, Zacharin M, Oexle K, Marcelino J, Suwairi W, Heeger S, Sabatakos G, Apte S, Adkins WN, Allgrove J, Arslan-Kirchner M, Batch JA, Beighton P, Black GC, Boles RG, Boon LM, Borrone C, Brunner HG, Carle GF, Dallapiccola B, De Paepe A, Floege B, Halfhide ML, Hall B, Hennekam RC, Hirose T, Jans A, Juppner H, Kim CA, Keppler-Noreuil K, Kohlschuetter A, LaCombe D, Lambert M, Lemyre E, Letteboer T, Peltonen L, Ramesar RS, Romanengo M, Somer H, Steichen-Gersdorf E, Steinmann B, Sullivan B, Superti-Furga A, Swoboda W, van den Boogaard MJ, Van Hul W, Vikkula M, Votruba M, Zabel B, Garcia T, Baron R, Olsen BR, Warman ML. LDL receptor-related protein 5 (LRP5) affects bone accrual and eye development. Cell. 2001; 107:513–523. [PubMed: 11719191]
30. Angers S, Moon RT. Proximal events in Wnt signal transduction. Nat. Rev. Mol. Cell Biol. 2009; 10:468–477. [PubMed: 19536106]

31. zur Nieden NI, Price FD, Davis LA, Everitt RE, Rancourt DE. Gene profiling on mixed embryonic stem cell populations reveals a biphasic role for beta-catenin in osteogenic differentiation. Mol. Endocrinol. 2007; 21:674–685. [PubMed: 17170073]
32. Hughes K, Nikolakaki E, Plyte SE, Totty NF, Woodgett JR. Modulation of the glycogen synthase kinase-3 family by tyrosine phosphorylation. EMBO J. 1993; 12:803–808. [PubMed: 8382613]
33. Wang QM, Fiol CJ, DePaoli-Roach AA, Roach PJ. Glycogen synthase kinase-3 beta is a dual specificity kinase differentially regulated by tyrosine and serine/threonine phosphorylation. J. Biol. Chem. 1994; 269:14566–14574. [PubMed: 7514173]
34. Case N, Rubin J. Beta-catenin--a supporting role in the skeleton. J. Cell. Biochem. 2010; 110:545–553. [PubMed: 20512915]
35. Lochhead PA, Kinstrie R, Sibbet G, Rawjee T, Morrice N, Cleghon V. A chaperone-dependent GSK3beta transitional intermediate mediates activation-loop autophosphorylation. Mol. Cell. 2006; 24:627–633. [PubMed: 17188038]
36. Jin EJ, Lee SY, Choi YA, Jung JC, Bang OS, Kang SS. BMP-2-enhanced chondrogenesis involves p38 MAPK-mediated down-regulation of Wnt-7a pathway. Mol. Cells. 2006; 22:353–359. [PubMed: 17202865]
37. Itasaki N, Hoppler S. Crosstalk between Wnt and bone morphogenic protein signaling: a turbulent relationship. Dev. Dyn. 2010; 239:16–33. [PubMed: 19544585]
38. Zhang M, Yan Y, Lim YB, Tang D, Xie R, Chen A, Tai P, Harris SE, Xing L, Qin YX, Chen D. BMP-2 modulates beta-catenin signaling through stimulation of Lrp5 expression and inhibition of beta-TrCP expression in osteoblasts. J. Cell. Biochem. 2009; 108:896–905. [PubMed: 19795382]
39. Nakashima A, Katagiri T, Tamura M. Cross-talk between Wnt and bone morphogenetic protein 2 (BMP-2) signaling in differentiation pathway of C2C12 myoblasts. J. Biol. Chem. 2005; 280:37660–37668. [PubMed: 16150699]
40. Hai B, Yan X, Voutetakis A, Zheng C, Cotrim AP, Shan Z, Ding G, Zhang C, Xu J, Goldsmith CM, Afione S, Chiorini JA, Baum BJ, Wang S. Long-term transduction of miniature pig parotid glands using serotype 2 adeno-associated viral vectors. J. Gene Med. 2009; 11:506–514. [PubMed: 19326368]
41. Lebherz C, Auricchio A, Maguire AM, Rivera VM, Tang W, Grant RL, Clackson T, Bennett J, Wilson JM. Long-term inducible gene expression in the eye via adeno-associated virus gene transfer in nonhuman primates. Hum. Gene Ther. 2005; 16:178–186. [PubMed: 15761258]
42. Podsakoff G, Wong KK Jr, Chatterjee S. Efficient gene transfer into nondividing cells by adeno-associated virus-based vectors. J. Virol. 1994; 68:5656–5666. [PubMed: 8057446]
43. Han Z, Zhong L, Maina N, Hu Z, Li X, Chouthai NS, Bischof D, Weigel-Van Aken KA, Slayton WB, Yoder MC, Srivastava A. Stable integration of recombinant adeno-associated virus vector genomes after transduction of murine hematopoietic stem cells. Hum. Gene Ther. 2008; 19:267–278. [PubMed: 18303957]
44. Subramanian K, Geraerts M, Pauwelyn KA, Park Y, Owens DJ, Muijtjens M, Ulloa-Montoya F, Jiang Y, Verfaillie CM, Hu WS. Isolation procedure and characterization of multipotent adult progenitor cells from rat bone marrow. Methods Mol. Biol. 2010; 636:55–78. [PubMed: 20336516]
45. Reyes M, Lund T, Lenvik T, Aguiar D, Koodie L, Verfaillie CM. Purification and ex vivo expansion of postnatal human marrow mesodermal progenitor cells. Blood. 2001; 98:2615–2625. [PubMed: 11675329]
46. Ng ES, Davis RP, Azzola L, Stanley EG, Elefanty AG. Forced aggregation of defined numbers of human embryonic stem cells into embryoid bodies fosters robust, reproducible hematopoietic differentiation. Blood. 2005; 106:1601–1603. [PubMed: 15914555]
47. Grieger JC, Choi VW, Samulski RJ. Production and characterization of adeno-associated viral vectors. Nat. Protoc. 2006; 1:1412–1428. [PubMed: 17406430]
48. Chang MC, Ko CC, Douglas WH. Preparation of hydroxyapatite-gelatin nanocomposite. Biomaterials. 2003; 24:2853–2862. [PubMed: 12742723]
49. Kasper FK, Young S, Tanahashi K, Barry MA, Tabata Y, Jansen JA, Mikos AG. Evaluation of bone regeneration by DNA release from composites of oligo(poly(ethylene glycol) fumarate) and

cationized gelatin microspheres in a critical-sized calvarial defect. J. Biomed. Mater. Res. A. 2006; 78:335–342. [PubMed: 16639744]

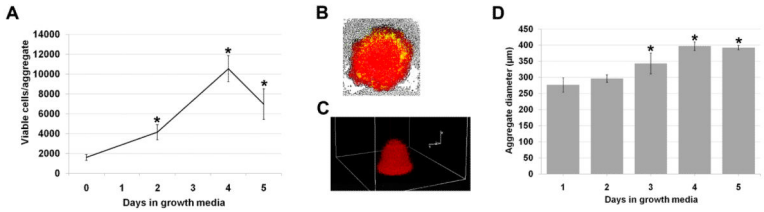

Figure 1.

Rat MAPC expansion and viability during 3D aggregate culture. (a) Cell proliferation in the aggregate during 5 days in growth media. Data are shown as mean ±SD of eight independent experiments. (b) Cell viability under fluorescence microscopy in one 3D aggregate using a non-fluorescent compound that changes to a red fluorescent color when cells are viable and metabolically active and changes to green when cells are damaged or dead. The image shown is a merge of three images taken with bright field, TRITC and FITC filters. (c) Three-dimensional rendered image showing viable cells (red) in a 3D aggregate under fluorescence microscopy. (d) Aggregate growth in diameter during 5 days in growth media. Data are shown as mean ±SD of five independent experiments. *$p<0.01$ when statistically compared to baseline (day 0 or 1).

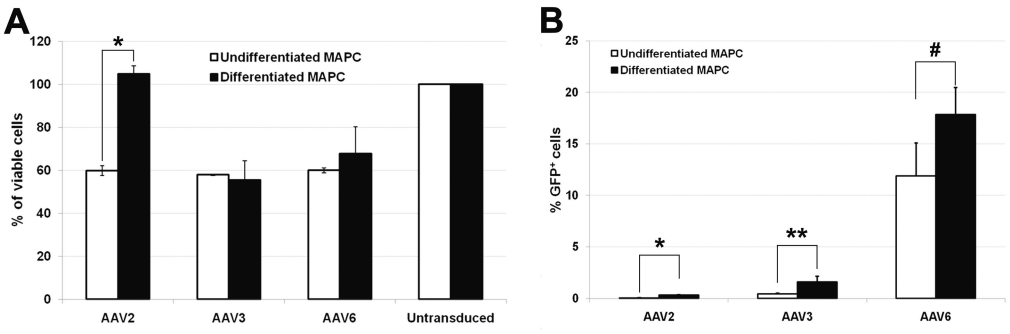

Figure 2.

Cell viability and transduction efficiency with AAV-GFP serotypes 2, 3, and 6 using rMAPC 3D culture system. Percentage of viable undifferentiated and osteogenically differentiated rMAPC (OD-MAPC) 72h after transduction with AAV-GFP serotype 2, 3, and 6 (a) when compared to untransduced cells (100%). Transduction efficiency after 72h in undifferentiated and differentiated MAPC measured by the percentage of cells expressing GFP vector (b). *p≤0.01, **p≤0.05, and #p=0.06, when statistically compared undifferentiated versus differentiated MAPC. Data are shown as mean ±SD of three independent experiments.

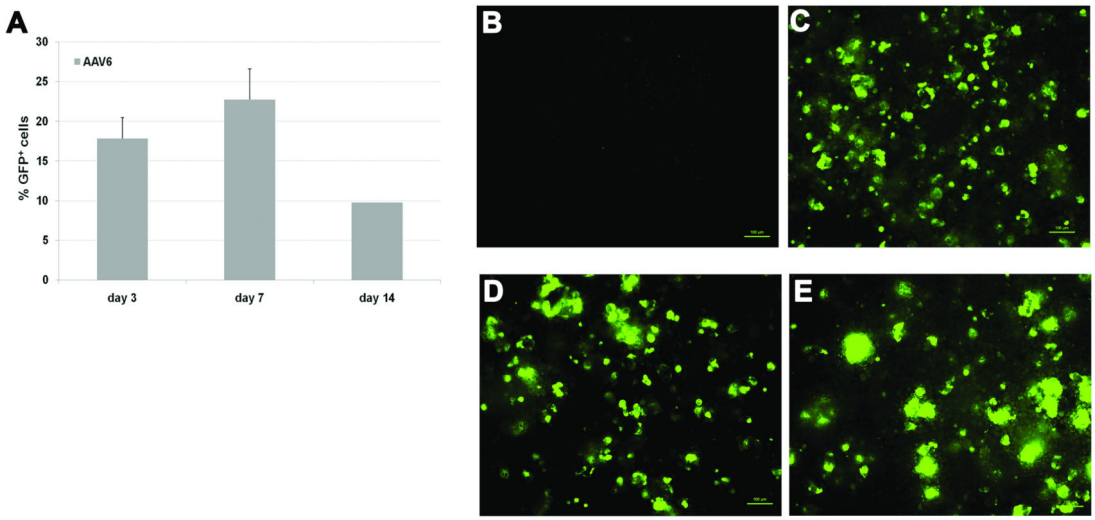

Figure 3.

Transduction efficiency and GFP expression on AAV6-transduced rMAPC after in vitro osteogenic differentiation. Number of GFP^+ rMAPC cells after 3, 7 and 14 days of vector transfer at MOI 100 (a). GFP expression on untransduced differentiated MAPC (b), and on AAV6-GFP-transduced cells 4 days (c), 10 days (d), 14 days (e) after vector transfer at MOI 100. Data are shown as mean ±SD of three independent experiments.

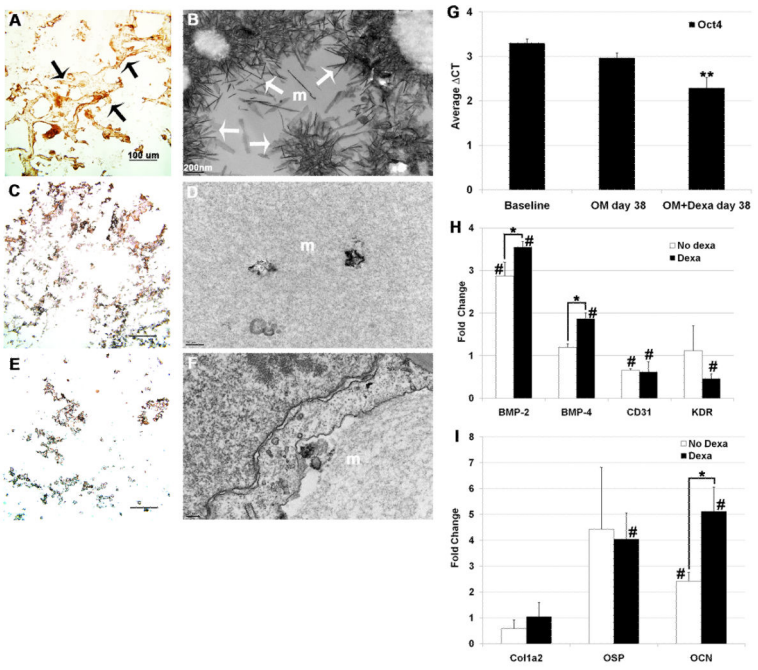

Figure 4.

Phenotypic and genotypic characterization of cell/matrices from 3D rMAPC cultures after 38 days of osteogenic differentiation. Aggregate cultures supplemented with: osteogenic media (OM) with dexamethasone (a-b), OM without dexamethasone (c-d), and basal media without osteogenic supplements and without dexamethasone (e-f). Matrices were immunostained with collagen type I antibody (a,c,e) showing a immunoreactive matrix network (black arrows). Matrices (m) visualized under transmission electron microscopy (b,d,f) showing large mineralization areas with spindle-like and plate-like crystals (white arrows). mRNA expression of specific markers at the MAPC 3D aggregate differentiation (g-i). MAPC-specific markers (g), mesoderm-specific markers (h) and mid to late bone-specific markers (i). Fold change was normalized to house-keeping genes and compared to baseline levels. Dexa: dexamethasone. **p<0.05 when statistically compared to both **Δ**CT at baseline and at OM day 38 of differentiation; *p<0.05 when statistically compared; #p<0.05 when statistically compared to baseline level. Data are shown as mean ±SD of three independent experiments.

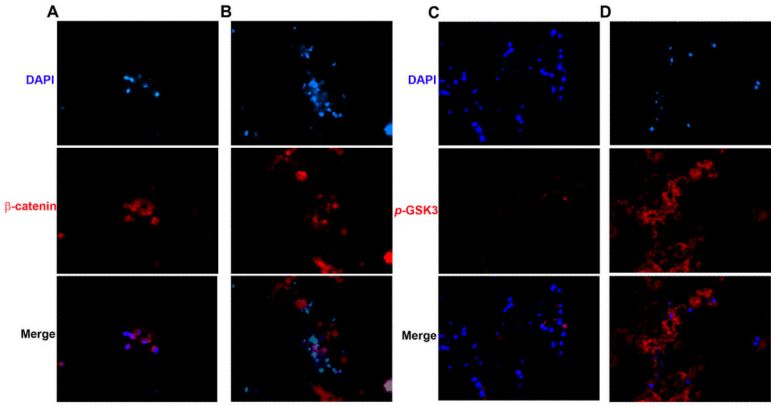

Figure 5.

β-catenin nuclear translocation (left) and *p*-GSK3 cellular localization (right) in rMAPC aggregate cultures in the presence and absence of dexamethasone in OM media after 38 days of osteogenic differentiation. Immunostained matrices from cultures with dexamethasone (a,c), and without dexamethasone (b,d). β-catenin immunoreactivity in red (a,b) and *p*-GSK3 immunoreactivity in red (c,d). Blue: nuclear DAPI, Magnification: 400x.

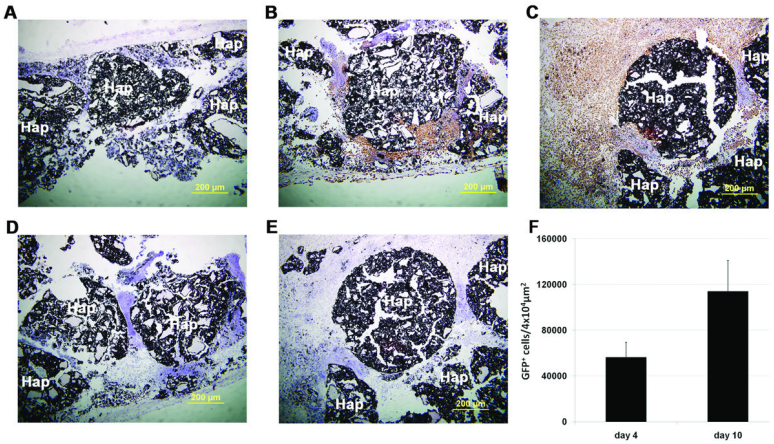

Figure 6.

"In vivo" tracing of osteogenic-differentiated rMAPC cells after AAV6-GFP transduction in a calvaria bone CSD formation model. Macro-porous 3D hydroxyapatite-based scaffolds carried untransduced cells (a) or AAV6-GFP-transduced cells (b-e) and GFP expression was visualized by immunohistochemistry with anti-GFP antibody after 4 days (b) and 10 days (c) "in vivo" and with isotype IgG antibody after 4 (d) and 10 days (e). Sections were stained with DAB chromogen and counterstained with hematoxylin. Quantification of rMAPC-GFP$^+$ cells "in vivo" (f) by light microscopy counting, mean from 5 technical replicates. Hap: hydroxyapatite-based biomaterial. Nuclei counterstained with hematoxylin. Magnification: 100x.

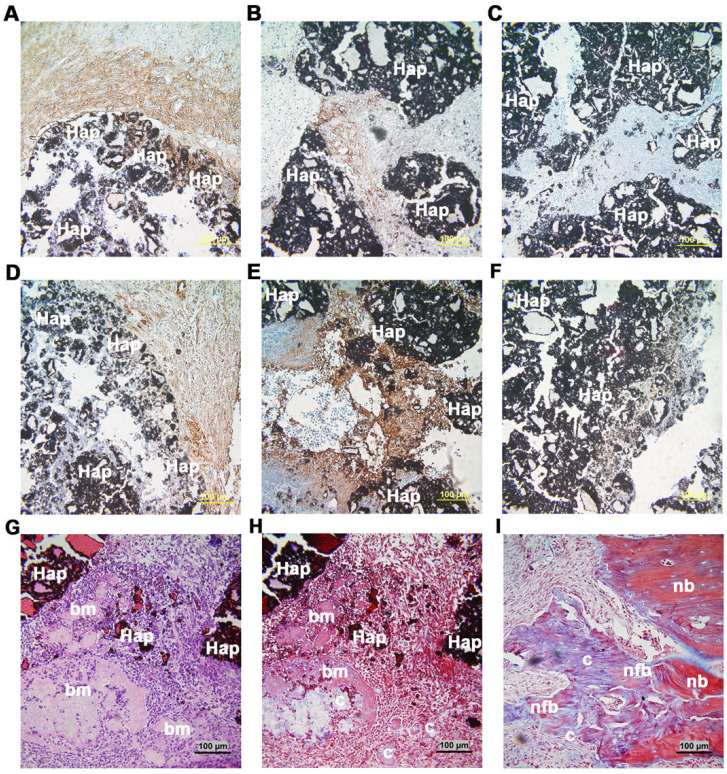

Figure 7.

Expression of osteogenic markers and newly formed bone tissue 10 days after “in vivo” implantation of AAV6-GFP-transduced OD-rMAPCs in a calvaria bone regeneration CSD model. Osteogenically differentiated rMAPCs (OD-rMAPCs treated with dexamethasone) were either untransduced (a,d) or transduced with AAV6-GFP vector (b,c,e-i) and were loaded into macro-porous 3D hydroxyapatite-based scaffolds (Hap) before implantation. Expression of osteopontin (a,b) and osteocalcin (d,e) was visualized by immunohistochemistry with anti-osteopontin and anti-osteocalcin primary antibodies and with isotype IgG antibody for those markers respectively (c,f). Nuclei counterstained with Alcian blue (a-f). In Figures g-i: formation of bone-like matrix (bm), collagenous matrix (c) in the macro-porous areas, and formation of newly formed bone (nfb) at native bone-scaffold interface can be visualized using hematoxylin-eosin (g) and Masson’s Trichrome (h-i) staining. These stains were used to assess bone-like and collagen matrix formation between the hydroxyapatite (Hap) biomaterials. bm: bone-like matrix; c: collagenous matrix; nfb: newly formed bone; nb: native bone; Magnification: 200x.

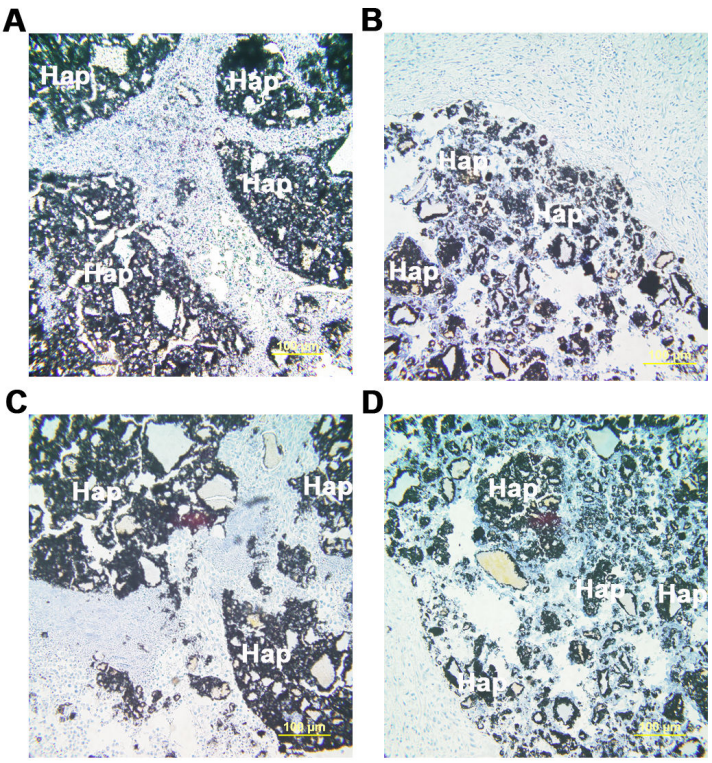

Figure 8.

Expression of the stem cell intracellular marker Oct4, 10 days after “in vivo” implantation of rMAPCs in a bone critical-size defect (CSD). Osteogenically differentiated rMAPCs (OD-rMAPCs) transduced with AAV6-GFP vector (a,c) and untransduced (b,d) were loaded into hydroxyapatite-based scaffolds (Hap) before implantation. Expression of Oct4 (a, b) was visualized by immunohistochemistry with anti-Oct4 primary antibody and with isotype IgG antibody (c,d) plus DAB chromogen (brown staining). Nuclei counterstained with Alcian blue. Magnification: 200x.